







Article

Equivalent Consumption Minimization Strategy Based on Belt Drive System Characteristic Maps for P0 Hybrid Electric Vehicles

Shailesh Hegde ^{1,*}, Angelo Bonfitto ¹, Renato Galluzzi ^{1,2}, Luis M. Castellanos Molina ¹, Nicola Amati ¹
and Andrea Tonoli ¹

¹ Center for Automotive Research and Sustainable Mobility, Department of Mechanical and Aerospace Engineering, Politecnico di Torino, 10129 Turin, Italy

² School of Engineering and Sciences, Tecnológico de Monterrey, Mexico City 14380, Mexico

* Correspondence: shailesh.hegde@polito.it

Abstract: A P0 system is used in hybrid automobiles to improve engine economy and performance. An essential element of the P0 system for effectively transmitting power to the drive train is the belt drive system (BDS). The features of electric machine (EM) and internal combustion engines (ICE) are taken into account by standard energy management systems, such as the equivalent consumption minimization strategy (ECMS). In order to maximize the effectiveness of the P0 system, this work provides a novel formulation of the ECMS, which considers the power loss map of the BDS in addition to the characteristic maps of EM and ICE. A test bench is built up to characterize the BDS, and it is verified using an open-loop Hardware in the Loop (HIL) in the WLTP driving cycle. To find the most appropriate equivalence factors for the ECMS, which would ordinarily be tuned through trial and error, a genetic algorithm (GA) is used. With regard to the standard ECMS, the proposed methodology intends to reduce fuel usage and CO₂ emissions. Two belts in BDS were tested in the WLTP to achieve CO₂ savings of 1.1 and 0.9 [g/km], indicating the enhancement of system performance by using the BDS power loss maps in ECMS.

Keywords: equivalent consumption minimization strategy; belt drive system characterization; genetic algorithm; HEV-P0



Citation: Hegde, S.; Bonfitto, A.; Galluzzi, R.; Molina, L.M.C.; Amati, N.; Tonoli, A. Equivalent Consumption Minimization Strategy Based on Belt Drive System Characteristic Maps for P0 Hybrid Electric Vehicles. *Energies* **2023**, *16*, 487. <https://doi.org/10.3390/en16010487>

Academic Editor: Gianpiero Colangelo

Received: 7 December 2022

Revised: 23 December 2022

Accepted: 26 December 2022

Published: 2 January 2023



Copyright: © 2023 by the authors. Licensee MDPI, Basel, Switzerland. This article is an open access article distributed under the terms and conditions of the Creative Commons Attribution (CC BY) license (<https://creativecommons.org/licenses/by/4.0/>).

1. Introduction

The need for reducing the impact of global mobility on the environment and the subsequent strict limits and regulations on vehicle emissions have forced a paradigm shift in automotive technology, especially in the powertrain. Alternative architectures have gained traction in the automotive market, with sales shifting away from pure internal combustion engine (ICE) layouts and toward electric vehicles (EVs) and hybrid electric vehicles (HEVs). In this context, HEVs represent an intermediate solution between conventional combustion and electric power sources. As a matter of fact, while meeting the regulatory demands, HEVs are efficient and well accepted by a large slice of users who are still skeptical about the complete electric transition given the high costs, limited range, and long charging periods [1–4]. Many types of HEVs are now present in the market. They all exploit ICE and one or more electric machines (EMs) and can be classified into micro, mild, full, or plug-in, based on the rated power and off-vehicle charging possibilities. The EMs provide traction torque to the vehicle in motor mode, while they recuperate the braking energy in generator mode. Additionally, EMs could be used as an alternator to recharge the battery by absorbing the additional power produced by the ICE in the so-called load shifting mode. Another classification, from P0 to P5, is based on the position of EMs along the driveline [5–8], as illustrated in Figure 1.

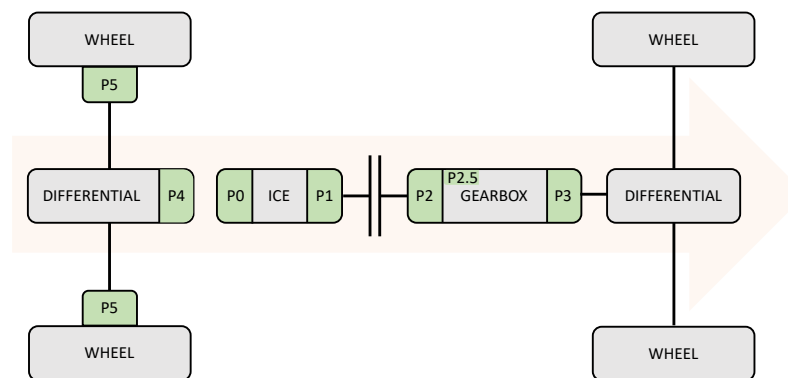


Figure 1. HEV architecture classification based on the position of the electric machine.

It is well known that a substantial part of the management of HEVs is devoted to the supervision of energy flows. When extracting energy from the ICE rather than from batteries, it is crucial to improve the overall vehicle efficiency. In general, the supervisory controller manages energy based on single or multiple objectives, such as minimizing fuel consumption, emissions, drivetrain efficiency, extending battery life by avoiding overcharging and undercharging, and optimizing gear-shifting strategy [7]. Based on objectives, various energy management control strategies were formulated in the past and are broadly classified into two categories: model-based and rule-based approaches. Model-based approaches include numerical methods, such as genetic algorithm (GA) [9,10], improved particle swarm optimization (PSO) [11] and dynamic programming [12]. Some analytical methods included in the model-based approach are Pontryagin's Minimum Principle [13], model predictive control (MPC) [14,15], nonlinear model predictive control [16], equivalent consumption minimization strategy (ECMS) [13,17,18], and adaptive equivalent consumption minimization strategy (AECMS) [19]. Rule-based methods, on the other hand, make use of heuristic approaches [6], rule-based optimal control [20], and fuzzy logic controller [21]. Rule-based approaches do not depend on the model but on the knowledge and experience of the designer. Furthermore, the solutions can be calibrated to correspond to those obtained from offline optimal solutions, such as dynamic programming. Additional techniques exploit artificial intelligence, such as neural networks, which are typically used to recognize the driving pattern and produce the power split command [22,23]. Further examples of these techniques are found in [24] and for charging electric vehicles with renewable energy sources in [25].

Few model-based techniques require prior knowledge of the whole driving cycle to solve the optimization problem and therefore cannot be used in real-world applications. On the other hand, rule-based methods rely on the instantaneous vehicle speed, torque request, and battery state of charge to produce the torque splitting command. They are inherently causal and simple to implement on hardware for real-time applications.

ECMS can be found as an intermediate solution between rule- and model-based approaches, since it produces an instantaneous optimal local torque splitting without the prior knowledge of a full driving cycle and is computationally inexpensive for hardware deployment. It is based on the computation of instantaneous optimal splitting between fuel and electrical energy. This is achieved through the minimization of an index that is given by the sum of the real and virtual fuel consumption. Fuel/electrical energy equivalence is obtained by means of a couple of parameters, called equivalence factors that convert the electric consumption into equivalent fuel consumption both in the case of boosting and generation. The typical approach to define these parameters is by trial-and-error methods. As an alternative, a shooting method [13] exploits the bi-section procedure that iteratively approaches the best solution starting from an arbitrary one. It is valid for the selection of the discharging mode equivalence only and has limitations when high accessory loads have to be considered in the optimization. To deterministically find the best-suited pair of equivalence factors, a GA is exploited in [26]. The authors proposed the method in a

previous paper, demonstrating that GA-ECMS always guarantees an optimal solution, even in the case of heavy accessory load in mild hybrid architectures, when the shooting method is no longer valid because it does not guarantee charge sustaining. The performance of energy management system (EMS) is highly influenced by the accuracy of the reference vehicle model. Thus, the subsystems of the vehicle, such as the power source, transmission, wheels, coast-down factors, etc., need to be modeled in a very accurate way. In particular, the computation of the optimal operating point in the standard ECMS formulation is strictly dependent on knowledge of the efficiency map of the EM and the ICE's brake specific fuel consumption (BSFC) map. The goal of this work is to re-formulate ECMS by including the efficiency of the belt drive system (BDS) in a parallel P0 HEV. P0 is the layout where the alternator is replaced by EM on the front-end accessory drive and is coupled to the ICE through a belt drive system (BDS). In this architecture, braking energy recovery is possible but limited by ICE drag and belt losses. In this powertrain, BDS losses are significant and depend on the drive layout, belt material, preload, and operating conditions in terms of torque and speed request. BDS transmission losses are quite significant and are not considered in typical ECMS. Here, the proposal is to provide this information with BDS power loss map along the torque speed characteristics, with positive and negative values of torque that is when the EM works as a motor or as a generator, respectively.

From the performance point of view, the overall vehicle efficiency is higher since the BDS loss characteristic is considered by the controller as a map, which is absent in the standard energy management system. The ECMS equivalence factors are designed through the adoption of a genetic algorithm, both for charge and discharge modes. The method is tested on a P0 HEV, exploiting experimental power loss maps of the BDS and using two different belts in the BDS to evaluate the robustness of the approach. The validation is conducted with a Hardware in the Loop (HIL) setup, where a test bench is reproducing the BDS with reference signals extracted in simulation for the World Harmonized Light Vehicle Test Procedure (WLTP) driving cycle. Then, the crankshaft torque measured on the test bench is compared to the simulation results using BDS experimental efficiency maps. The major contributions of the work are:

1. A novel formulation of ECMS takes into account the efficiency of BDS as a map. This map is obtained experimentally with a dedicated test bench. To the best of the authors' knowledge, this approach is not present in the literature to date. Based on the vehicle architecture, the expected CO₂ savings are around 1 g/km.
2. A GA is used as optimization method to compute in a deterministic way the equivalence factors of the ECMS. This method reduces calibration time and identifies the optimal solution, which would otherwise be determined through trial and error.

To this end, the remainder of this work is structured as follows: Section 2 describes the vehicle modeling and formulation of the proposed control strategy. Section 2.1 presents the vehicle model and parameters used in the Matlab/Simulink environment, belt drive system characterization, and HIL validation. Section 2.2 describes the procedure for the design of the energy management system considering the BDS power loss maps (ECMS-BDS) and the setup of GA for tuning the equivalence factors. Section 3 presents the performance of ECMS-BDS against standard ECMS. Finally, Section 4 draws conclusions and discusses future work.

2. Method

This section describes the vehicle model and parameters used for simulations, as well as the controller's design.

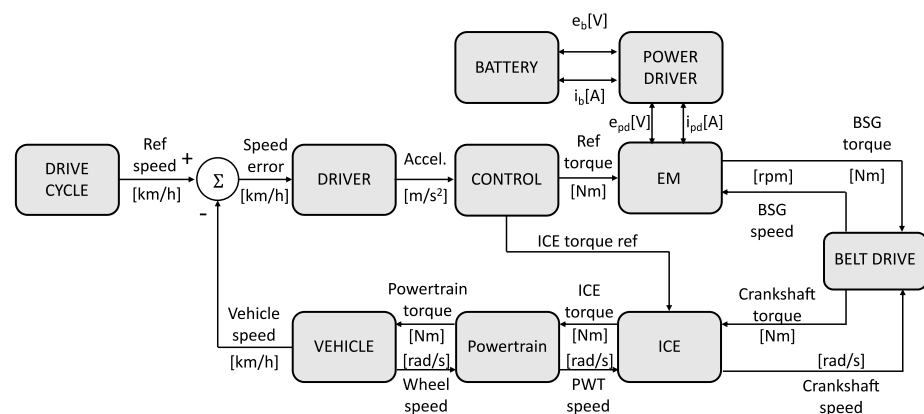
2.1. Vehicle Model

A 2-Ton sedan passenger vehicle is studied in this research. It is equipped with a P0 mild hybrid powertrain architecture. The power of EM is 13 kW and nominal energy of the battery is 1.2 kWh. The vehicle has a 12 speed automatic transmission. Table 1 contains data on the vehicle's key parameters.

Table 1. Vehicle parameters.

Parameters	Values	Unit
Mass	2000	[kg]
Drag coefficient	0.25	[-]
Engine Characteristic	Diesel 238 Nm	[-]
Electric machine characteristics	BLDC 13 kW	[-]
Battery nominal voltage	48	[V]
Battery Capacity	25	[Ah]
Belt drive transmission ratio	3	[-]
Transmission	12-speed automatic	[-]
Final drive ratio	3.1	[-]
Wheel radius	0.31	[m]
Rolling resistance coefficient	0.02	[-]

The vehicle is simulated using a forward model, as shown in Figure 2. At every time step, the driver, whose behavior is reproduced by a Proportional-Integral controller, compares the vehicle's current speed with the reference speed imposed by the driving cycle (i.e., WLTP) and calculates the torque demand. The EMS splits the torque demand between the ICE, EM, and brakes according to the control strategy described in Section 2.2. Another possible alternative to the forward model is a backward model, where the driver model is absent and the driving cycle speed is imposed as vehicle speed. Unlike the backward model, the forward model extensively considers vehicle dynamics. Moreover, the limitations in actuation delay and lag of the ICE and EM are considered in the vehicle model. Thus, the forward model has higher precision even if more computationally complex and expensive.

**Figure 2.** Vehicle forward model representation.

The electric machine is a brushless direct current electric motor (BLDC) with a peak power of 13 kW in boost and recuperation and a maximum torque of 50 Nm. The EM is modeled by the torque speed characteristic, efficiency map of the machine (Figure 3), and its inertia. The EM can be used to recover energy from braking and, during traction, it can assist the engine by providing a portion of the requested torque. Additionally, it can operate in generator mode to absorb the surplus torque generated by the engine, thus making the engine operate in the optimal region, in the so-called load shifting mode.

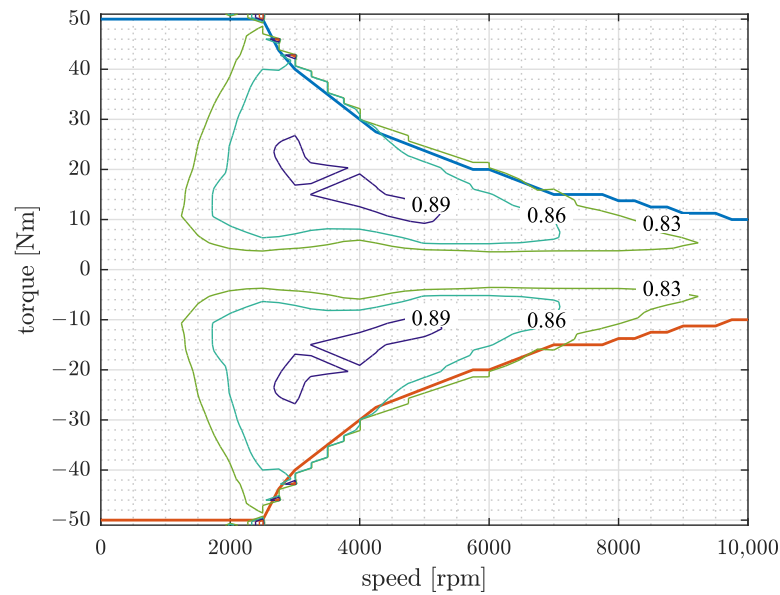


Figure 3. Torque/speed characteristic of the electric machine with an efficiency map.

The electric machine is powered by a 48 V battery pack, which acts as an energy buffer for the electrical energy recovered during recuperation and load shifting. Its state of charge (SOC) is calculated from the current extracted from or provided to the battery. The battery is modeled with an equivalent electric circuit composed of an ideal voltage source in series with an internal resistor. The open circuit voltage of the source varies with the SOC as follows:

$$V = V_0 \left(\frac{SOC}{1 - \beta \cdot (1 - SOC)} \right) \quad (1)$$

where V_0 is the open circuit voltage at full battery capacity and β is a characteristic parameter. The battery SOC is always kept within a boundary to preserve health. The SOC is updated as follows [27]:

$$SOC(t) = - \frac{I_{batt}(t)}{Q_{batt,0}} \quad (2)$$

where $Q_{batt,0}$ is the maximum battery charge capacity, and $I_{batt}(t)$ is the current flowing to or from the battery. For a deeper level of battery behaviour representation, a better battery behavior model could be obtained by taking into account the health and degradation of batteries [28–30]. The ICE block in the model consists of a BSFC map, which is used to calculate fuel consumption based on the torque and speed of the ICE, as illustrated in Figure 4.

The two subsystems, EM and ICE, are connected through a BDS. In this study, it has a constant transmission ratio, and its power loss is obtained through an experimental characterization, which is described in the following section. The characterization of a BDS is discussed in the following subsection. Moreover, the total torque transferred through the powertrain block takes into account the efficiency, transmission ratio, and inertia of the gearbox, differential, and wheels. Finally, the vehicle block, which is a 3DOF model, calculates the current vehicle speed based on the vehicle dynamics.

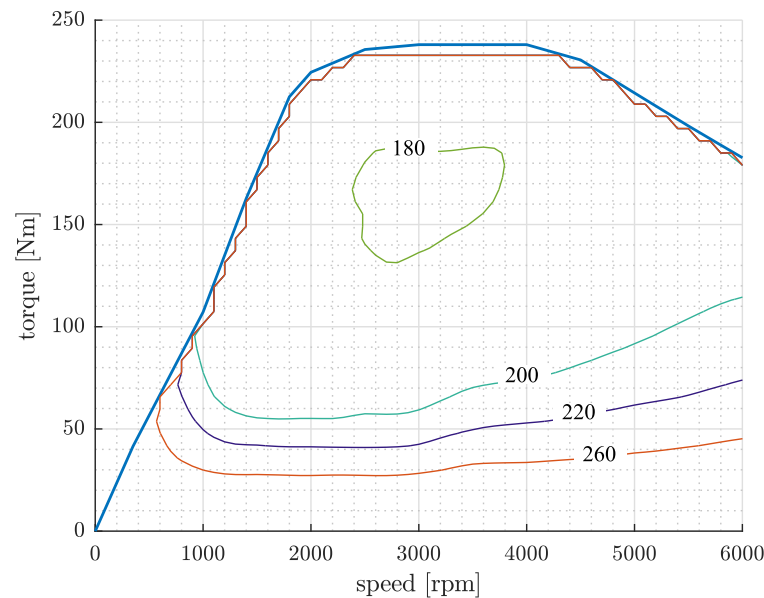


Figure 4. Engine brake specific fuel consumption (BSFC) map [g/kWh].

Belt Drive System Characterization

In this research, two different belts, named Belt A and Belt B, will be used to assess the robustness of the proposed controller. The BDS is characterized on a dedicated test bench [31], the layout of which is shown in Figure 5. It is based on a full electric configuration exploiting two EMs. These are Bosch Rexroth brushless motors from the IndraDyn-H series and replicate the behavior of the ICE crankshaft and the BSG. Each EM is controlled by a dedicated IndraDrive inverter. The modular power section is completed by two Bosch Rexroth inverters (HMS01.1N-W0210 and HMS01.1N-W0070). The crankshaft behavior is emulated with a 38 kW motor with a maximum speed of 12 krpm and a maximum torque of 320 Nm. The test bench is equipped with sensors to measure the system variables. The position feedback of both motors is accomplished with two Heidenhain ERM 2984 magnetic encoders (192 lines of resolution, 1 Vpp sinusoidal incremental signals, a maximum rotational speed of 47,000 rpm and a power supply of 5 Volts). The values of torque for the two electric machines are calculated from the corresponding current feedback values in the direct and quadrature axes. The angular positions of the tensioner arms are measured through two Kuebler KIS incremental encoders (2500 lines of resolution). Each encoder is hinged to its respective tensioner pulley employing a two-link kinematic arrangement. This mechanism is designed to follow and reproduce the angular displacement of the tensioner arms. The tension in both belt spans is measured on the two idler pulleys, which are equipped with Magtrol DB radial load cells (a maximum force of 750 N). Their output is fed through an HBM Force Measurement System amplifier. A power supply (HMV01.1R-W0065-A-07 by Bosch Rexroth) powers both inverters which are connected to the same DC BUS. The main feature of such a supply unit is the possibility of power regeneration at the mains, meaning that the power produced by one of the two motors acting as the alternator is given back to the network. A dSpace MicroLabBox Platform is used to support a human-machine interface that commands the inverters and acquires the signals of interest. This system communicates with a host PC via Ethernet and with both motor inverters through CAN Open protocol. The inverters receive torque or speed reference values from the MicroLabBox device. In turn, they yield the actual measurements of speed and current of both motors. In the dSpace platform, the 14-bit analog channels are used to read the load cell amplified signals, while the tensioner arm encoders are processed by direct capture inputs.

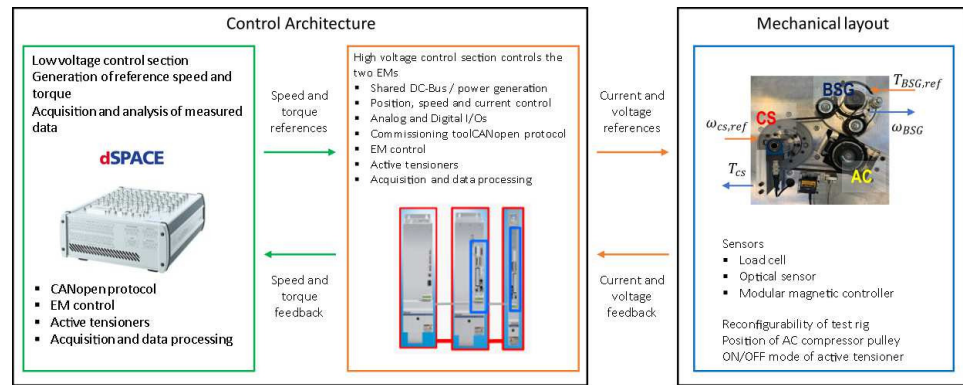


Figure 5. Test bench for the belt drive system characterization and key signal interfaces with the controller platform.

The belt slip at the BSG pulley is obtained from the measurements as:

$$\sigma(t) = 1 - \frac{\omega_{BSG}(t)}{\omega_{BSG}(T_{CS} = 0)} \quad (3)$$

The power at crankshaft (P_{CS}) and BSG (P_{BSG}) are obtained as:

$$\begin{aligned} P_{CS}(t) &= T_{CS}(t)\omega_{CS}(t) \\ P_{BSG}(t) &= T_{BSG}(t)\omega_{BSG}(t) \end{aligned} \quad (4)$$

where T_{CS} is the crankshaft torque, T_{BSG} is the BSG torque, ω_{CS} is the crankshaft speed and ω_{BSG} is the BSG speed. The dissipated power (P_{loss}) is:

$$P_{loss}(t) = P_{CS}(t) + P_{BSG}(t) \quad (5)$$

The transmission efficiency in boosting (η_{boost}) and braking mode (η_{brake}) is calculated as:

$$\begin{aligned} \eta_{boost} &= -\frac{P_{CS}(t)}{P_{BSG}(t)} \\ \eta_{brake} &= -\frac{P_{BSG}(t)}{P_{CS}(t)} \end{aligned} \quad (6)$$

The experimental tests were conducted for crankshaft speeds of 800, 2000, and 3000 rpm and BSG load ranging from -30 to $+30$ Nm. The results obtained from the experimental characterization of BDS are illustrated in Figures 6 and 7, where the 3D representations depict the slip, power loss and efficiency of the transmission in the three rows, respectively, when varying the value of ω_{CS} (in the columns). All the values are obtained as functions of the belt preload and torque of the BSG. The efficiency mapping over the crankshaft speed range is obtained by interpolating the different values of ω_{CS} in experiments. Figures 8 and 9 illustrate the system behavior of both belts in the case of three different belt preloads: 180 N (green line), 350 N (blue line), and 600 N (red line) at 2000 rpm (ω_{CS}). The two subplots report power loss and transmission efficiency. The top subplot indicates that, as expected, the power loss is strictly dependent on the belt preload. The increasing preload produces more power loss. Additionally, the bottom subplot gives a quantification of the transmission efficiency's dependence on the belt preload and the BSG torque.

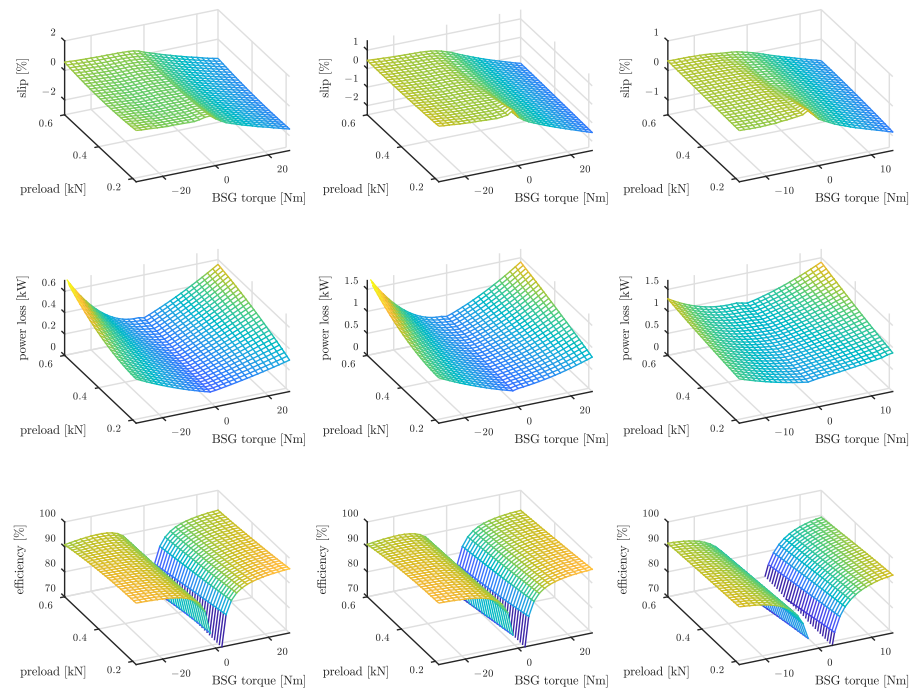


Figure 6. Characteristic maps of BDS with Belt A. 1st row: Slip. 2nd row: Power loss. 3rd row: transmission efficiency. The columns indicate three different values of the crankshaft speed (ω_{CS}). 1st column: 800 rpm, 2nd column: 2000 rpm, 3rd column: 3000 rpm.

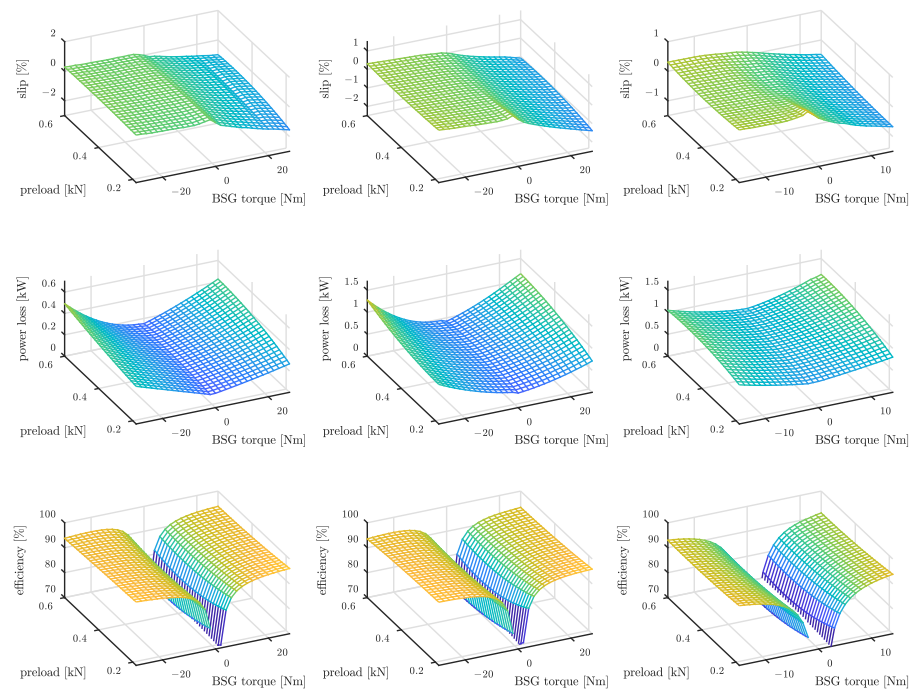


Figure 7. Characteristic maps of BDS with Belt B. 1st row: Slip. 2nd row: Power loss. 3rd row: transmission efficiency. The columns indicate three different values of the crankshaft speed (ω_{CS}). 1st column: 800 rpm, 2nd column: 2000 rpm, 3rd column: 3000 rpm.

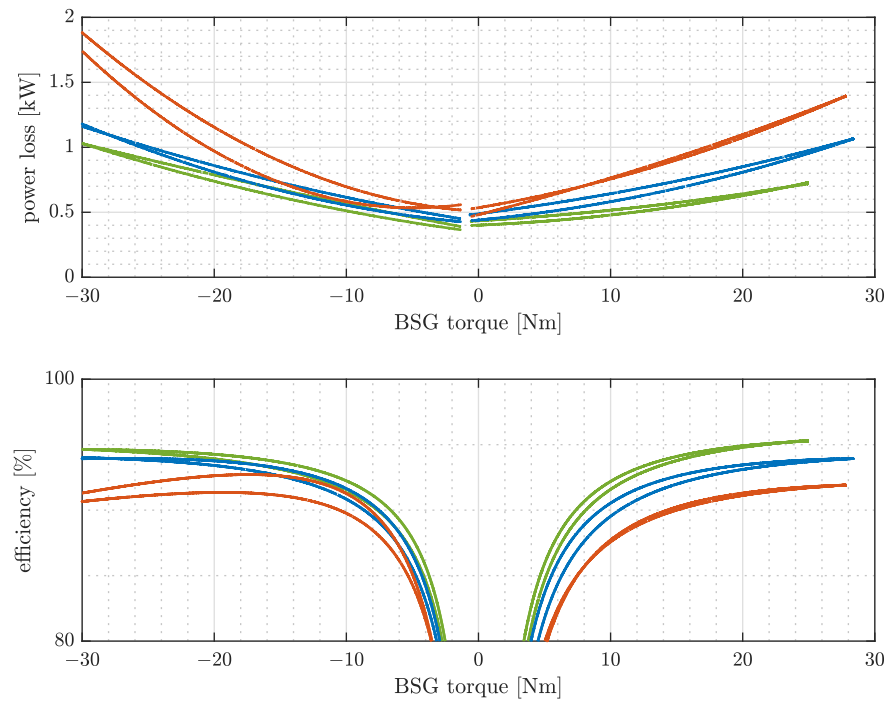


Figure 8. 2D characteristic maps of BDS with Belt A at the speed (ω_{CS}) equal to 2000 rpm and at different belt preloads: 180 N (green line), 350 N (blue line) and 600 N (red line). 1st row: power loss. 2nd row: transmission efficiency.

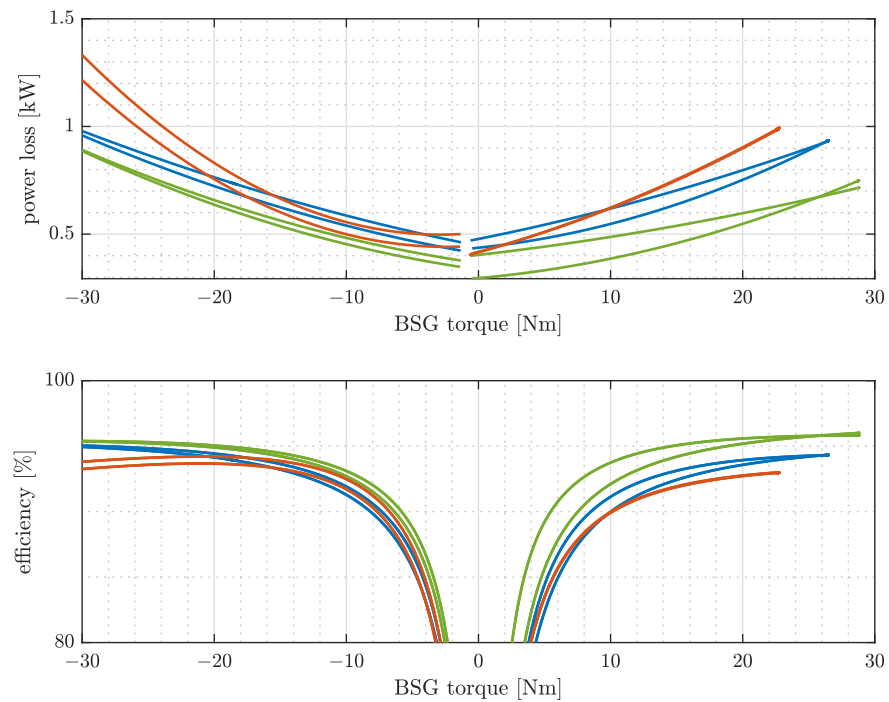


Figure 9. 2D characteristic maps of BDS with Belt B at the speed (ω_{CS}) equal to 2000 rpm and at different belt preloads: 180 N (green line), 350 N (blue line) and 600 N (red line). 1st row: power loss. 2nd row: transmission efficiency.

In order to validate the BDS characterization with more dynamic speed and torque profiles, a HIL simulation was setup, as shown in Figure 10. The interpolated power loss map of the BDS from experimentation was used in simulation. An open-loop HIL was performed using simulation-recorded reference signals, namely $\omega_{CS,ref}$ and $T_{BSG,ref}$. In HIL testing, the MicroLabBox hardware platform was used to send reference signals to

the EM and BDS via CAN bus. When compared to the crankshaft torque measured in HIL testing, the actual crankshaft torque observed in simulation is quite accurate, as shown in Figure 11.

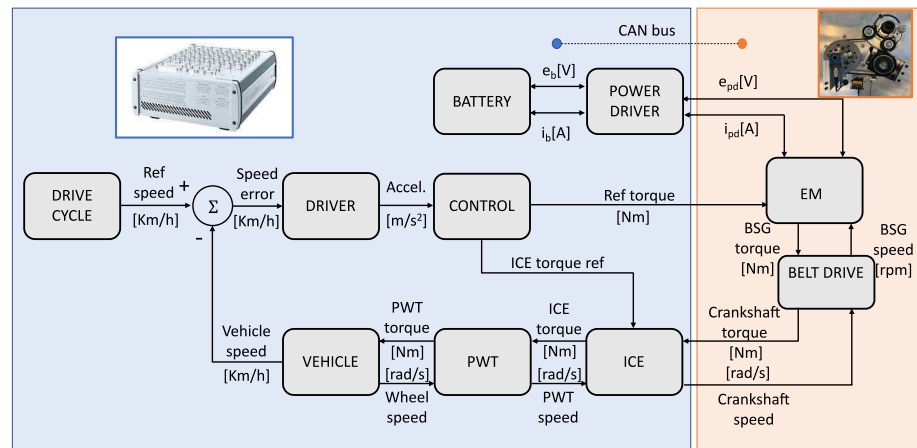


Figure 10. Block diagram of HIL setup to validate the characterization of BDS.

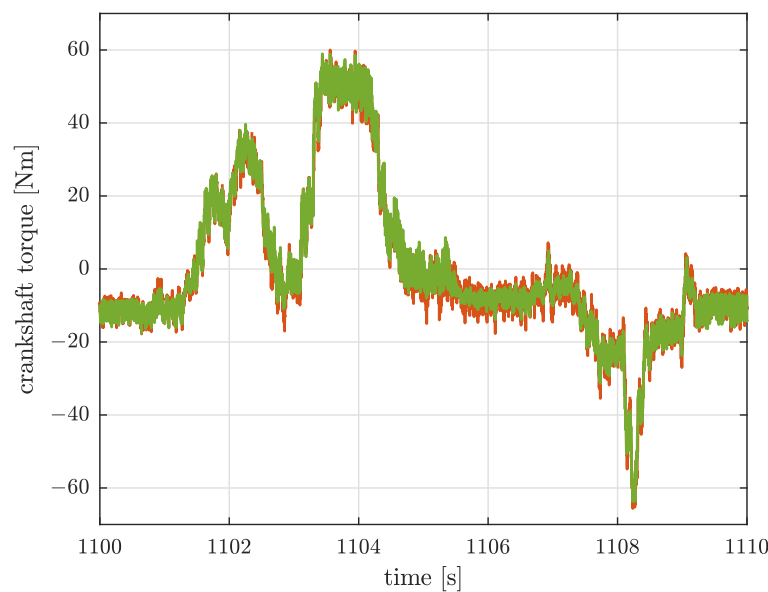


Figure 11. Crankshaft torque comparison. Orange line: experimental results with HIL setup; green line: numerical results.

The obtained experimental characterization of the BDS is included in the proposed formulation of the ECMS to consider the BDS efficiency. This helps to improve the system efficiency and overall vehicle performance.

2.2. Energy Management System Design

The objective of the EMS is to provide the reference signals to powertrain, guarantee charge sustaining, and minimize fuel consumption and emissions. The baseline EMS used in this study is the standard ECMS. Standard ECMS computes at every time step the optimal power to be provided by ICE and the power from or to the battery. The original ECMS formulation and equations are available in [13,27]. The ECMS provides an instantaneous splitting torque ratio between ICE and EM by allocating a cost (equivalence factor) to the electrical power with respect to ICE fuel consumption. These equivalence factors are indicated as S_{ch} (charging) and S_{disch} (discharging) and typically they are calibrated with a trial-and-error approach. Here, a GA is proposed to identify the best-suited equivalence

factors to minimize fuel consumption and achieve a charge sustaining performance. To this end, a novel reformulation of ECMS is proposed, where the belt power loss maps in addition to the ICE BSFC and EM efficiency maps are used to compute the optimal torque splitting. In the following subsections, the reformulation of the ECMS and the method for determining equivalence factors are presented.

2.2.1. Equivalent Consumption Minimization Strategy (ECMS)

The primary goal of ECMS is to achieve optimal torque splitting between ICE and EM while also ensuring charge sustaining behavior. To obtain the final SOC balance in the driving cycle, all the energy must be provided by the ICE, and the battery acts as an energy buffer. As a result, the energy extracted from the battery for traction must be replenished through braking recuperation or ICE load shifting regeneration.

The adopted process flow for the ECMS-based EMS is shown in the flow chart illustrated in Figure 12. EMS provides references to ICE, EM, and brakes in traction and braking conditions. In traction, the EMS could select one of the following modes: pure ICE mode, pure EM mode, or ICE with EM boost assistance or regeneration.

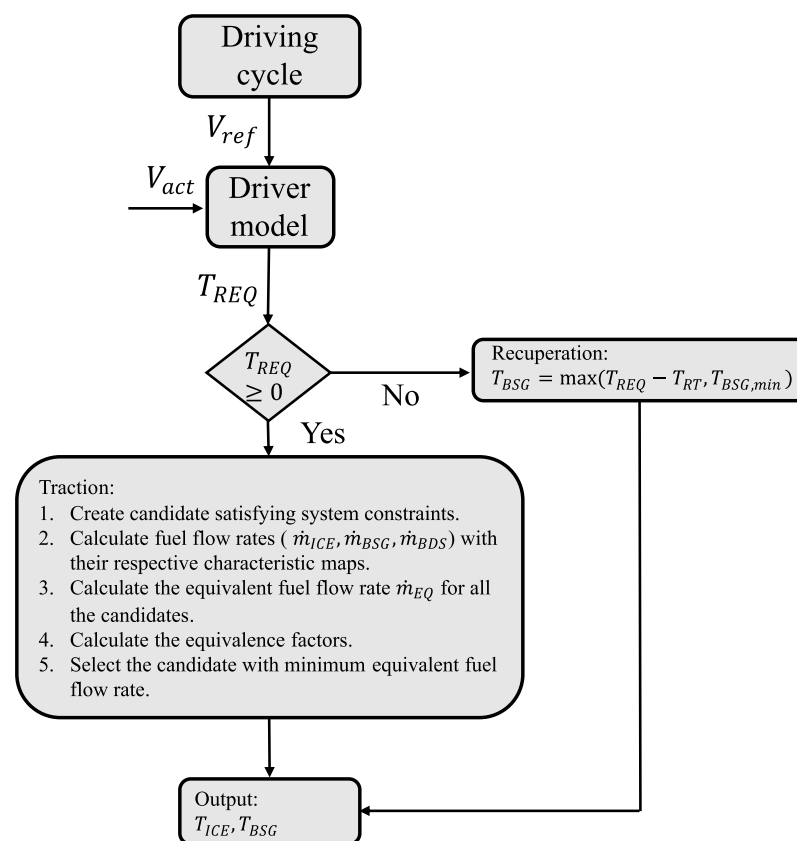


Figure 12. ICE/EM splitting decision flow based on ECMS supervision.

Knowing system states, namely, that the torque requested by the driver (T_{REQ}), the angular speed of the ICE (ω_{CS}), angular speed of the electric machine (ω_{BSG}), and the battery state of charge (SOC), ECMS determines an instantaneous local optimal solution, $u(t)$. The ratio of BSG torque to total requested torque is expressed as $u(t)$:

$$u(t) = \frac{T_{BSG}(t)}{T_{REQ}(t)}, u(t) \in \left[\frac{T_{BSG,min}(\omega_{BSG}(t))}{T_{REQ}(t)}, \dots, \frac{T_{BSG,max}(\omega_{BSG}(t))}{T_{REQ}(t)} \right] \quad (7)$$

$$T_{ICE}(t) = (1 - u(t)) \cdot T_{REQ}(t)$$

$$T_{BSG}(t) = u(t) \cdot T_{REQ}(t)$$

The set of decision variables ($u(t)$) are obtained by satisfying the system constraints as follows:

$$\begin{aligned} T_{REQ}(t) &= T_{ICE}(t) + T_{BSG}(t) \\ 0 &\leq T_{ICE}(t) \leq T_{ICE,max}(\omega_{CS}(t)) \\ T_{BSG,min}(\omega_{BSG}(t)) &\leq T_{BSG}(t) \leq T_{BSG,max}(\omega_{BSG}(t)) \\ SOC_{min} &\leq SOC(t) \leq SOC_{max} \end{aligned} \quad (8)$$

where $T_{BSG,min}$ and $T_{BSG,max}$ are the EM's maximum torque in generator and motor modes, respectively. The decision variable, $u(t)$, is discretized into a finite number of candidates. During traction, $u(t)$ less than zero means the EM is operating in generator mode, and $u(t)$ greater than zero indicates that the electric machine is in motor mode. For every time step, an equivalent fuel rate is computed for every candidate as follows:

$$\begin{aligned} \dot{m}_{EQ}(t) &= \dot{m}_{ICE}(t) + \dot{m}_{BSG}(t) + \dot{m}_{BDS}(t), \quad \text{for } u(t) \geq 0 \\ \dot{m}_{EQ}(t) &= \dot{m}_{ICE}(t) + \dot{m}_{BSG}(t) + \dot{m}_{BDS}(t), \quad \text{for } u(t) < 0 \end{aligned} \quad (9)$$

where \dot{m}_{ICE} is the fuel flow rate of the ICE, \dot{m}_{BSG} and \dot{m}_{BDS} are the virtual fuel flow rate of an BSG and BDS, respectively. The virtual fuel flow rate of the BSG and BDS is calculated as follows:

$$\begin{aligned} \dot{m}_{BSG}(t) &= S_{dischg} \cdot \frac{P_{elec,mot,BSG}(t)}{Q_{LHV}}, \quad \text{for } u(t) \geq 0 \\ \dot{m}_{BSG}(t) &= S_{chg} \cdot \frac{P_{elec,gen,BSG}(t)}{Q_{LHV}}, \quad \text{for } u(t) < 0 \end{aligned} \quad (10)$$

$$\begin{aligned} \dot{m}_{BDS}(t) &= S_{bp} \cdot \frac{P_{loss,mot,BDS}(t)}{Q_{LHV}}, \quad \text{for } u(t) \geq 0 \\ \dot{m}_{BDS}(t) &= S_{bp} \cdot \frac{P_{loss,gen,BDS}(t)}{Q_{LHV}}, \quad \text{for } u(t) < 0 \end{aligned} \quad (11)$$

where Q_{LHV} is the lower heating value of the fuel, $P_{elec,mot,BSG}(t)$ and $P_{elec,gen,BSG}(t)$ are the electrical powers of the BSG in motor and generator mode, respectively. $P_{loss,mot,BDS}(t)$ and $P_{loss,gen,BDS}(t)$ are the power loss of the BDS in motor and generator mode, respectively. S_{dischg} and S_{chg} are the equivalence factors in battery discharging and charging, respectively. S_{bp} is the equivalence factor for the BDS. S_{bp} is set to zero in standard ECMS. The equivalence factors in battery discharging and charging are calculated as follows:

$$\begin{aligned} S_{dischg} &= S_{GA,dischg} + \frac{S_{GA,dischg}}{4} \cdot (SOC_{ref} - SOC(t)), \quad \text{for } u(t) \geq 0 \\ S_{chg} &= S_{GA,chg} + \frac{S_{GA,chg}}{4} \cdot (SOC_{ref} - SOC(t)), \quad \text{for } u(t) < 0 \end{aligned} \quad (12)$$

where $S_{GA,dischg}$ and $S_{GA,chg}$ is the equivalence factor, which is the outcome of genetic algorithm optimization, and SOC_{ref} is the reference battery SOC. In this study, the initial SOC of the battery is used as the reference SOC for every simulation.

The equivalence factor of BDS is calculated as follows:

$$\begin{aligned} S_{bp} &= K_{bp} \cdot \left(1 + \frac{P_{loss,mot,BDS}(\omega_{BSG}(t)) - P_{loss,mot,BDS,min}(\omega_{BSG}(t))}{P_{loss,mot,BDS,max}(\omega_{BSG}(t)) - P_{loss,mot,BDS,min}(\omega_{BSG}(t))} \right) \\ K_{bp} &= \frac{P_{BSG,mot,max}(\omega_{BSG}(t))}{(P_{loss,mot,BDS,max}(\omega_{BSG}(t)) + P_{loss,mot,BDS,min}(\omega_{BSG}(t)))/2} \end{aligned} \quad (13)$$

where $P_{loss,mot,BDS,max}(\omega_{BSG}(t))$ and $P_{loss,mot,BDS,min}(\omega_{BSG}(t))$ is the maximum and minimum BDS power loss, respectively for the given $\omega_{BSG}(t)$, $P_{BSG,mot,max}(\omega_{BSG}(t))$ is the

maximum available power in BSG, and $P_{loss,mot,BDS}(\omega_{BSG}(t))$ is the BDS power loss for all the candidates. The $u(t)$ corresponding to the minimum of $m_{EQ}(t)$ is selected as a solution.

In braking, the torque requested by the driver is fulfilled by the combinations of the action: hydraulic brakes, ICE resisting torque produced during fuel cut-off causing engine overrun, and EM in generator mode:

$$\begin{aligned} T_{ICE}(t) &= 0 \\ T_{BSG}(t) &= \max(T_{REQ}(t) - T_{RT}(t), T_{BSG,min}(\omega_{BSG}(t))) \\ T_{BRAKE}(t) &= \min(T_{REQ}(t) - T_{BSG}(t), 0) \end{aligned} \quad (14)$$

where $T_{BSG,min}(\omega_{BSG}(t))$ is the maximum torque available from the EM in generator mode, $T_{REQ}(t)$ is the torque requested from the driver, $T_{BSG}(t)$ is the BSG torque reference, $T_{BRAKE}(t)$ is the torque reference to the hydraulic brakes, and $T_{RT}(t)$ is the ICE resisting torque.

2.2.2. ECMS Equivalence Factors Selection with Genetic Algorithm

The selection of S_{chg} and S_{dischg} obtained through a GA-based optimiser. GA is based on evolutionary theory to search for a global optimal solution. An initial population consists of a finite feasible solution known as chromosomes, which are randomly created. A set of operators, namely crossover, mutation, and elitism, are exploited to reproduce the population every generation. The mutation and crossover reproduce the candidates from the previous generation either by merging or modifying the chromosomes. Elitism saves the best chromosomes from the current generation and passes them down to the next. Throughout the evolution, the fitness value of each candidate is calculated and ranked. The GA flow chart is shown in Figure 13, while design procedure is as follows:

1. The initial population with size 40 is generated with bounds of [0, ..., 4].
2. Vehicle model simulation is performed for every candidate. The output of the simulation is the fuel consumption [l/100 km] and SOC. They are used to evaluate the fitness value, F_{obj} as:

$$\begin{aligned} F_{obj} &= f_c + (SOC_{ref} - SOC_{final}) \cdot CF_a, \text{ if } |\Delta SOC| \leq \Delta SOC_{threshold} \\ F_{obj} &= f_c + (SOC_{ref} - SOC_{final}) \cdot CF_p, \text{ if } |\Delta SOC| > \Delta SOC_{threshold} \\ CF_p &= \text{sign}(SOC_{ref} - SOC_{final}) \cdot 0.03 \end{aligned} \quad (15)$$

where f_c is the consumed fuel in l/100km, ΔSOC is the difference between initial and final SOC, $CF_a = 0.014$ is the correction factor obtained from the fitting shown in Figure 14, and $\Delta SOC_{threshold} = 2\%$ is the limit in SOC variation for GA fitness value. The CF_p is a big number to heavily penalize the fitness value for a big deviation in (SOC).

3. The best set of chromosomes is chosen (a stochastic uniform selection procedure is used).
4. Survivor selection is based on elitism to retain the potential best solution for the next generation (the elite count is 2).
5. The new population is generated by a crossover procedure.
6. The mutation operation (Gaussian distribution) is performed to widen the search space.
7. The fitness value of the new population is evaluated. Steps 2–7 are recursively iterated till the stopping criterion is met (50 generations).

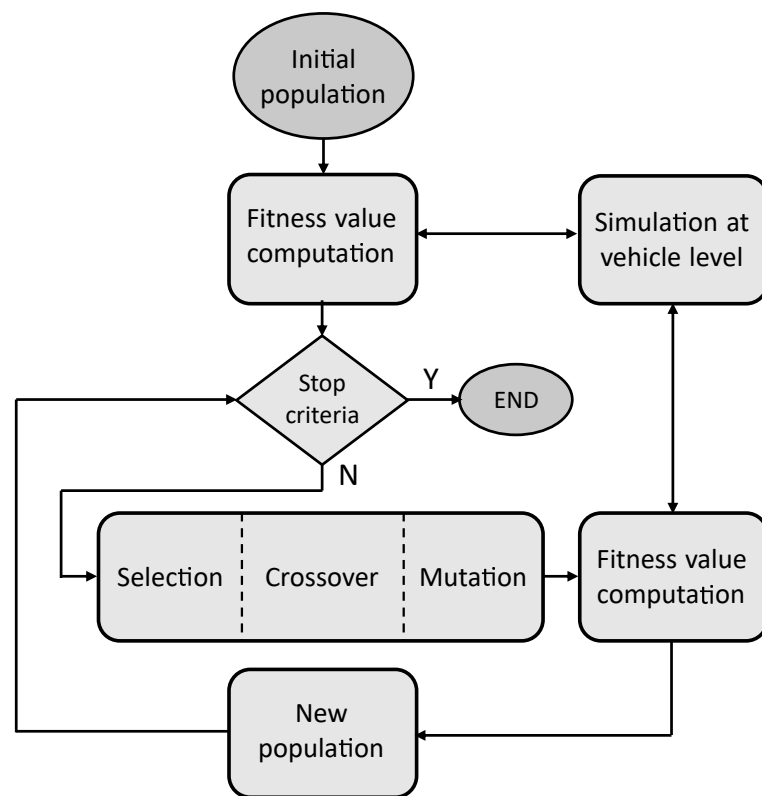


Figure 13. Method for the deterministic selection of optimal charge and discharge equivalence factors.

For any given values of S_{chg} and S_{dischg} computed by the candidates of GA, the SOC_{final} and $SOC_{initial}$ may not be the same. For a fair and true evaluation of fitness value, a correction factor (CF_a) is used to convert the ΔSOC to its fuel equivalent. A linear regression approximates the correlation between the dependent variable which are the fuel consumption and the difference between final and reference SOC, respectively. The data set was generated through simulation using S_{chg} and S_{dischg} values which are generated randomly. The linear regression model is expressed as:

$$f_c = f_{corr} + CF_a \cdot (SOC_{final} - SOC_{ref}) \quad (16)$$

where f_{corr} is the corrected fuel consumption that takes SOC deviation into account, and f_c is the fuel consumption at the end of a driving cycle. To determine the fitness value in GA, the aforementioned equation is rearranged as follows:

$$f_{corr} = f_c + CF_a \cdot (SOC_{ref} - SOC_{final}) \quad (17)$$

The regression model fitting is shown in Figure 14.

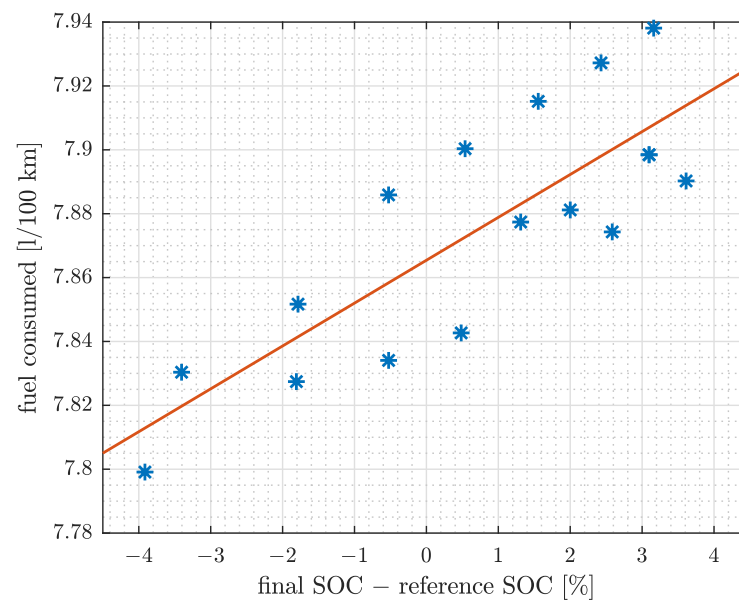


Figure 14. Correction factor for compensation of possible deviations in final SOC from reference SOC. Blue points: data recorded from simulations. Red line: interpolation function.

3. Results and Discussion

To evaluate the performance of the proposed method, the experimentally characterized BDS maps are used to model the BDS. The characteristic map of the BDS is included in the ECMS-BDS formulation. To tune the equivalence factors, a GA is employed. In this study, simulations are performed with two distinct belts, namely, Belt A and Belt B. The simulations are performed with the WLTP driving cycle. The benefits of ECMS-BDS is compared against the standard ECMS.

3.1. Simulation Results Using Belt A

In the case of Belt A, the BDS power loss map with a preload of 350 N was used for simulation. The equivalence factors of ECMS-BDS ($S_{GA,dischg} = 0.68$ and $S_{GA,chg} = 0.61$) and standard ECMS ($S_{GA,dischg} = 0.95$ and $S_{GA,chg} = 0.85$) were obtained from GA optimization. Figure 15 shows the time series plot of standard ECMS and ECMS-BDS, where the first and second rows represent ICE and BSG torque, respectively. The ECMS-BDS makes a different torque splitting decision than the standard ECMS. This is due to the fact that the ECMS-BDS includes the BDS map. As for the SOC, the third row of Figure 15 shows that the two controllers ensure charge sustaining.

The total energy of BSG in motor and generator mode, as well as total BDS losses over the WLTP driving cycle, are reported for the two controllers in Table 2. The energy provided by the BSG for boosting (motor mode) is higher in ECMS-BDS vs. standard ECMS (1372 [kJ] vs. 1245 [kJ]). In idle mode, the BDS losses are higher in standard ECMS vs. ECMS-BDS (364 [kJ] vs. 279 [kJ]). Though ECMS-BDS has higher losses in motor mode, it achieves an optimal splitting ratio between ICE and BSG, resulting in lower overall fuel consumption. The CO₂ emissions [g/km] for two controllers are reported in Table 3. The ECMS-BDS has lower CO₂ emissions (205.7 [g/km] vs. 204.6 [g/km]) for Belt A. The CO₂ savings of 1.1 [g/km] is achieved in Belt A layout.

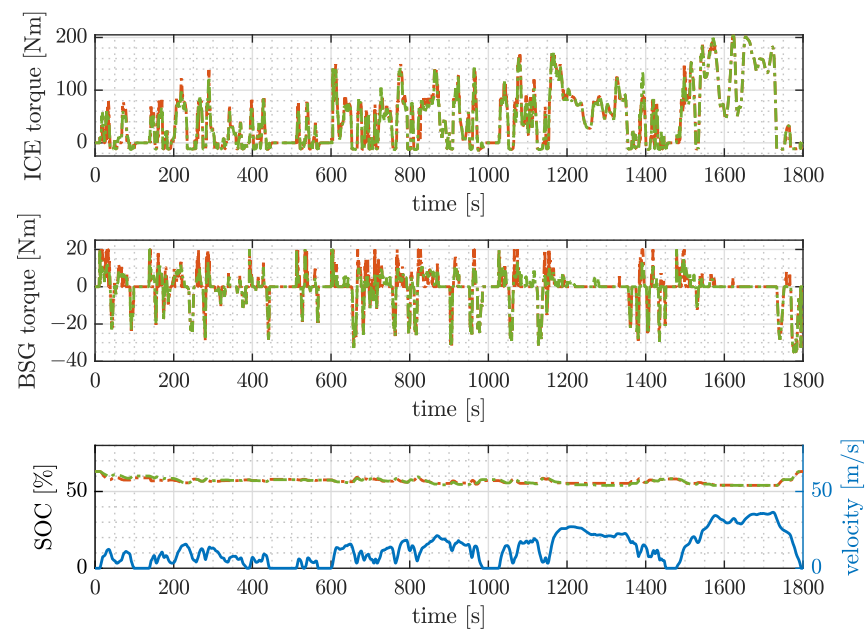


Figure 15. Simulation conducted on WLTP driving cycle with belt A. Orange line: ECMS standard. Green line: ECMS with BDS power loss maps. Top: torque provided by the ICE. Center: torque provided by the electric machine. Bottom: battery state of charge and vehicle speed profile (blue).

Table 2. Energy at subsystems – Belt A in WLTP driving cycle for standard ECMS and ECMS-BDS.

Subsystem	Modes	Energy [kJ] (Standard ECMS)	Energy [kJ] (ECMS-BDS)
BSG	Motor	1245	1372
	Generator	−2176	−2176
BDS losses	Motor	120	197
	Idle	364	279
	Generator	147	147

Table 3. CO₂ emission comparison of the considered controllers—Belt A.

Controller Type	CO ₂ Emissions [g/km]	CO ₂ Emission Savings [g/km]
Standard ECMS	205.7	−
ECMS-BDS	204.6	1.1

3.2. Simulation Results Using Belt B

Another simulation was performed using the Belt B power loss map with a preload of 350 N to test the effectiveness of the ECMS-BDS. The equivalence factors of ECMS-BDS ($S_{GA,dischg} = 0.72$ and $S_{GA,chg} = 0.63$) and standard ECMS ($S_{GA,dischg} = 0.92$ and $S_{GA,chg} = 0.81$) are obtained from GA optimization. According to Figures 8 and 9, Belt B is more efficient than Belt A (see the BDS losses in Table 2 and 4), resulting in lower overall CO₂ emissions in Belt B. The time series plot of standard ECMS and ECMS-BDS is shown in Figure 16. The plots of ICE torque and BSG torque are in the first and second rows, respectively. Because of distinguishable characteristics in both maps, torque splitting decisions in ECMS-BDS with Belt B differ from ECMS-BDS with Belt A.

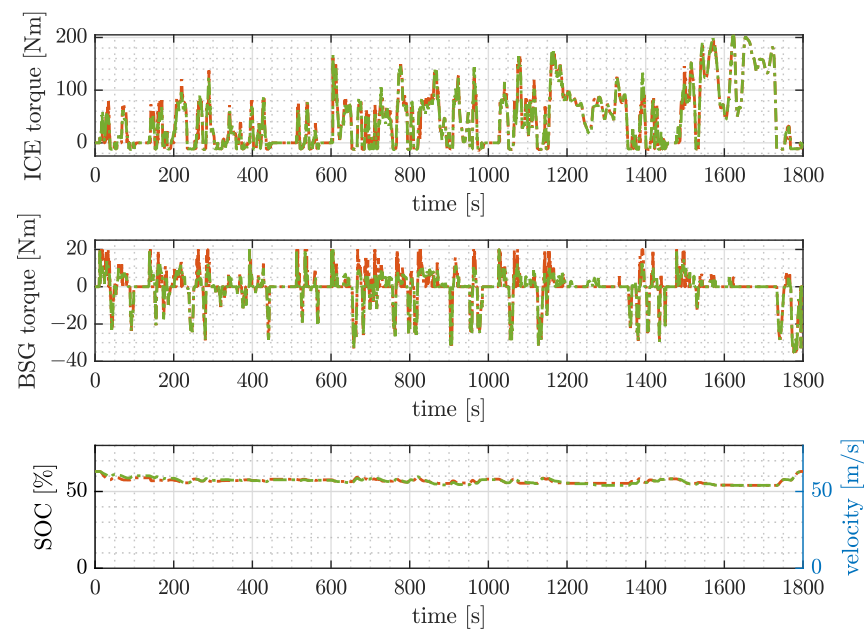


Figure 16. Simulation conducted on the WLTP driving cycle with belt B. Orange line: ECMS standard. Green line: ECMS with BDS power loss maps. Top: torque provided by the ICE. Center: torque provided by the electric machine. Bottom: battery state of charge and vehicle speed profile (blue).

The total energy of BSG in motor and generator mode, as well as total BDS losses over the WLTP driving cycle, are reported for the two controllers in Table 4. The energy provided by the BSG for boosting (motor mode) is higher in ECMS-BDS vs. standard ECMS (1395 [kJ] vs. 1295 [kJ]). In idle mode, the BDS losses are higher in standard ECMS vs. ECMS-BDS (259 [kJ] vs. 189 [kJ]). The CO₂ emissions [g/km] for two controllers are reported in Table 5. The ECMS-BDS has lower CO₂ emissions (203.6 [g/km] vs. 202.7 [g/km]) for Belt B layout. The CO₂ savings of 0.9 [g/km] is achieved in Belt B layout.

Table 4. Energy at subsystems—Belt B in WLTP driving cycle for standard ECMS and ECMS-BDS.

Subsystem	Modes	Energy [kJ] (Standard ECMS)	Energy [kJ] (ECMS-BDS)
BSG	Motor	1295	1395
	Generator	−2203	−2203
BDS losses	Motor	94	152
	Idle	259	189
	Generator	114	114

Table 5. CO₂ emission comparison of the considered controllers—Belt B.

Controller Type	CO ₂ Emissions [g/km]	CO ₂ Emission Savings [g/km]
Standard ECMS	203.6	−
ECMS-BDS	202.7	0.9

In the ECMS-BDS, the BSG provides higher energy with lower BDS losses, thus reducing the effort on the ICE. The equivalence factors yielded by GA optimization aid in finding the optimal torque splitting between the ICE and the BSG. The equivalence factors yielded by GA optimization aid in finding optimal torque splitting. Thus, an improvement of around 1 [g/km] of CO₂ is observed.

4. Conclusions

In this paper, a methodology for the performance optimization of a P0 system has been presented. The proposed methodology is a model-based energy flow supervisor (ECMS) that provides instantaneous optimal ICE/EM power splitting based on the power loss map of the belt drive system in an effort to reduce fuel consumption and, consequently, emissions. The paper discussed the experimental measurement of the BDS power loss maps on a dedicated test bench. Furthermore, the paper detailed the design of the supervisory controller, i.e., ECMS-BDS, and the tuning of the equivalence factors of ECMS-BDS using a genetic algorithm method. The HIL testing was setup to validate the performance of the experimentally characterized BDS maps. Finally, simulations using the WLTP driving cycle were performed to determine the benefits in terms of belt drive losses and CO₂ reduction. When compared to the standard ECMS approach, the proposed formulation saves 1.1 g/km of CO₂ for Belt A and 0.9 g/km for Belt B, respectively. The results analysis demonstrates the importance of incorporating the belt drive efficiency map into the supervisor optimal ICE/EM splitting procedure. In addition, the method provides a systematic design approach for a real-time energy flow supervisor. The highlights of the work are: (a) it uses belt drive power loss mapping; and (b) it is a deterministic approach that is not based on manual calibration through trial-and-error procedures.

Future objectives of this work include analyzing and developing a control strategy to reduce the harmonic torque and speed fluctuations, which can improve drivetrain stability and extend their service life. In addition, the incorporation of the BSG's temperature-based efficiency maps in the ECMS may result in additional improvements.

Author Contributions: Conceptualization, A.B., N.A. and A.T.; Data curation, S.H., R.G. and L.M.C.M.; Methodology, S.H., A.B., R.G. and L.M.C.M.; Project administration, A.B., N.A. and A.T.; Supervision, A.B., N.A. and A.T.; Validation, S.H., A.B., R.G. and L.M.C.M.; Writing—original draft, S.H.; Writing—review and editing, S.H., A.B., R.G., L.M.C.M., N.A. and A.T. All authors have read and agreed to the published version of the manuscript.

Funding: This research received no external funding.

Data Availability Statement: Data is not available due to restrictions.

Acknowledgments: This work was developed in the framework of the activities of the Interdepartmental Center for Automotive Research and Sustainable Mobility (CARS) at Politecnico di Torino (www.cars.polito.it, accessed on 6 December 2022).

Conflicts of Interest: The authors declare no conflict of interest.

Abbreviations

The following abbreviations are used in this manuscript:

BDS	Belt Drive System
ICE	Internal Combustion Engine
EVs	Electric Vehicles
EMS	Energy management system
HEVs	Hybrid Electric Vehicles
EM	Electric Machine
GA	Genetic Algorithm
ECMS	Equivalent Consumption Minimization Strategy
BSFC	Brake Specific Fuel Consumption
HIL	Hardware in the Loop
WLTP	World harmonized Light vehicles Test Procedure
BSG	Belt Starter Generator
BLDC	Brushless direct current electric motor
ECMS-BDS	Equivalent Consumption Minimization Strategy with belt drive system maps
SOC	State of Charge
V	Open circuit voltage

V_0	Open circuit voltage when battery is at full capacity
β	Battery characteristic parameter
P_{CS}	Power at ICE crankshaft
P_{BSG}	Power at BSG
T_{CS}, T_{ICE}	Torque of ICE crankshaft
T_{BSG}	Torque of BSG
ω_{CS}	Speed of ICE crankshaft
ω_{BSG}	Speed of BSG
P_{loss}	Dissipated power in BDS
η_{boost}	Transmission efficiency of belt drive system in boosting
η_{brake}	Transmission efficiency of belt drive system in recuperation
T_{REQ}	Torque requested by the driver
u	Ratio of BSG torque to total requested torque
$T_{ICE,max}$	Maximum ICE torque for a given speed
$T_{BSG,min}$	Minimum BSG torque for a given speed
$T_{BSG,max}$	Maximum BSG torque for a given speed
SOC_{min}	Lower limit of SOC
SOC_{max}	Upper limit of SOC
\dot{m}_{ICE}	Fuel flow rate of an engine
\dot{m}_{BSG}	Virtual fuel flow rate of the BSG
\dot{m}_{BDS}	Virtual fuel flow rate of the BDS
Q_{LHV}	Lower heating value of the fuel
$P_{elec,mot,BSG}$	Electrical power of the BSG in motor mode
$P_{elec,gen,BSG}$	Electrical power of the BSG in generator mode
$P_{loss,mot,BDS}$	Power loss of the BDS in motor mode
$P_{loss,gen,BDS}$	Power loss of the BDS in generator mode
S_{dischg}	Equivalence factor of ECMS in discharging of battery
S_{chg}	Equivalence factor of ECMS in charging of battery
SOC_{ref}	SOC reference
$S_{GA,dischg}$	Equivalence factor provided by genetic algorithm in discharging of battery
$S_{GA,chg}$	Equivalence factor provided by genetic algorithm in charging of battery
S_{bp}	Equivalence factor of the BDS
$P_{loss,mot,BDS}$	Power loss of the BDS in motor mode
$P_{loss,mot,BDS,min}$	Minimum power loss of the BDS in motor mode
$P_{loss,mot,BDS,max}$	Maximum power loss of the BDS in motor mode
$P_{BSG,mot,max}$	Maximum power of the BSG in motor mode
T_{BRAKE}	Torque reference to the hydraulic brakes
T_{RT}	ICE resisting torque
F_{obj}	Fitness value in genetic algorithm
f_c	Fuel consumption
SOC_{final}	Battery SOC at the end of a driving cycle
CF_a	Correction factor to correlate fuel consumption and SOC deviation
CF_p	Correction factor for heavy penalties
$\Delta SOC_{threshold}$	Limit in SOC variation for GA fitness value
ΔSOC	Deviation in battery state of charge
f_{corr}	Corrected fuel consumption

References

1. Communication from the Commission to the European Parliament, the Council, the European Economic and Social Committee and the Committee of the Regions ‘Fit for 55’: Delivering the EU’s 2030 Climate Target on the Way to Climate Neutrality. 2021. Available online: <https://eur-lex.europa.eu/legal-content/EN/TXT/?uri=CELEX:52021DC0550> (accessed on 6 December 2022).
2. EUR-Lex—32019R0631—EN—EUR-Lex. Doc ID: 32019R0631 Doc Sector: 3 Doc Title: Regulation (EU) 2019/631 of the European Parliament and of the Council of 17 April 2019 Setting CO₂ Emission Performance Standards for New Passenger Cars and for New Light Commercial Vehicles, and Repealing Regulations (EC) No 443/2009 and (EU) No 510/2011 (recast) (Text with EEA Relevance.) Doc Type: R Ustr_lan: En. Available online: <https://eur-lex.europa.eu/eli/reg/2019/631/oj> (accessed on 6 December 2022).

3. Nguyen, H.P.; Hoang, A.T.; Le, A.T.; Pham, V.V.; Tran, V.N. Learned experiences from the policy and roadmap of advanced countries for the strategic orientation to electric vehicles: A case study in Vietnam. *Energy Sources Part A Recovery Util. Environ. Eff.* **2020**, 1–10. [\[CrossRef\]](#)
4. Nguyen, H.P.; Hoang, A.T.; Nizetic, S.; Nguyen, X.P.; Le, A.T.; Luong, C.N.; Chu, V.D.; Pham, V.V. The electric propulsion system as a green solution for management strategy of CO₂ emission in ocean shipping: A comprehensive review. *Int. Trans. Electr. Energy Syst.* **2021**, 31, e12580. [\[CrossRef\]](#)
5. Liu, W. *Introduction to Hybrid Vehicle System Modeling and Control*; John Wiley & Sons, Inc.: Hoboken, NJ, USA, 2013. [\[CrossRef\]](#)
6. Guzzella, L.; Sciarretta, A. *Vehicle Propulsion Systems: Introduction to Modeling and Optimization*, 2nd ed.; Springer: Berlin/Heidelberg, Germany, 2007.
7. Biswas, A.; Emadi, A. Energy Management Systems for Electrified Powertrains: State-of-the-Art Review and Future Trends. *IEEE Trans. Veh. Technol.* **2019**, 68, 6453–6467. [\[CrossRef\]](#)
8. Khan, I.; Ruzimov, S.; Amati, N.; Tonoli, A. Study of the Impact of E-Machine in Hybrid Dual Clutch Transmission Powertrain. *Energies* **2022**, 15, 945. [\[CrossRef\]](#)
9. Denis, N.; Dubois, M.R.; Trovao, J.P.F.; Desrochers, A. Power Split Strategy Optimization of a Plug-in Parallel Hybrid Electric Vehicle. *IEEE Trans. Veh. Technol.* **2018**, 67, 315–326. [\[CrossRef\]](#)
10. Piccolo, A.; Ippolito, L.; zo Galdi, V.; Vaccaro, A. Optimisation of energy flow management in hybrid electric vehicles via genetic algorithms. In Proceedings of the 2001 IEEE/ASME International Conference on Advanced Intelligent Mechatronics, Proceedings (Cat. No.01TH8556), Como, Italy, 8–12 July 2001; Volume 1, pp. 434–439. [\[CrossRef\]](#)
11. Yi, F.; Lv, Z.; Liu, Y.; Liu, H. Fuzzy adaptive control strategy with improved PSO algorithm for parallel hybrid electric vehicle. *Int. J. Simul. Syst. Sci. Technol.* **2016**, 17. [\[CrossRef\]](#)
12. Kolmanovsky, I.; Siverguina, I.; Lygoe, B. Optimization of powertrain operating policy for feasibility assessment and calibration: Stochastic dynamic programming approach. In Proceedings of the 2002 American Control Conference (IEEE Cat. No.CH37301), Anchorage, AK, USA, 8–10 May 2002; Volume 2, pp. 1425–1430. [\[CrossRef\]](#)
13. Onori, S.; Serrao, L.; Rizzoni, G. *Hybrid Electric Vehicles*; SpringerBriefs in Electrical and Computer Engineering; Springer: London, UK, 2016. [\[CrossRef\]](#)
14. He, L.; Shen, T.; Yu, L.; Feng, N.; Song, J. A Model-Predictive-Control-Based Torque Demand Control Approach for Parallel Hybrid Powertrains. *IEEE Trans. Veh. Technol.* **2013**, 62, 1041–1052. [\[CrossRef\]](#)
15. Kermani, S.; Delprat, S.; Guerra, T.; Trigui, R.; Jeanneret, B. Predictive energy management for hybrid vehicle. *Control Eng. Pract.* **2012**, 20, 408–420. [\[CrossRef\]](#)
16. Borhan, H.; Vahidi, A.; Phillips, A.M.; Kuang, M.L.; Kolmanovsky, I.V.; Di Cairano, S. MPC-Based Energy Management of a Power-Split Hybrid Electric Vehicle. *IEEE Trans. Control Syst. Technol.* **2012**, 20, 593–603. [\[CrossRef\]](#)
17. Paganelli, G.; Guerra, T.M.; Delprat, S.; Santin, J.J.; Delhom, M.; Combes, E. Simulation and assessment of power control strategies for a parallel hybrid car. *Proc. Inst. Mech. Eng. Part D J. Automob. Eng.* **2000**, 214, 705–717. [\[CrossRef\]](#)
18. Gao, A.; Deng, X.; Zhang, M.; Fu, Z. Design and Validation of Real-Time Optimal Control with ECMS to Minimize Energy Consumption for Parallel Hybrid Electric Vehicles. *Math. Probl. Eng.* **2017**, 2017, 3095347. [\[CrossRef\]](#)
19. Rezaei, A. An Optimal Energy Management Strategy for Hybrid Electric Vehicles. Ph.D. Thesis, Michigan Technological University, Houghton, MI, USA, 2017. [\[CrossRef\]](#)
20. Torres, J.; Gonzalez, R.; Gimenez, A.; Lopez, J. Energy management strategy for plug-in hybrid electric vehicles. A comparative study. *Appl. Energy* **2014**, 113, 816–824. [\[CrossRef\]](#)
21. Khoucha, F.; Benbouzid, M.; Kheloui, A. An optimal fuzzy logic power sharing strategy for Parallel Hybrid Electric Vehicles. In Proceedings of the 2010 IEEE Vehicle Power and Propulsion Conference, Lille, France, 1–3 September 2010; pp. 1–5. [\[CrossRef\]](#)
22. Murphey, Y.L.; Park, J.; Kiliaris, L.; Kuang, M.L.; Masrur, M.A.; Phillips, A.M.; Wang, Q. Intelligent Hybrid Vehicle Power Control—Part II: Online Intelligent Energy Management. *IEEE Trans. Veh. Technol.* **2013**, 62, 69–79. [\[CrossRef\]](#)
23. Balan, G.; Arumugam, S.; Muthusamy, S.; Panchal, H.; Kotb, H.; Bajaj, M.; Ghoneim, S.S.M.; Kitmo. An Improved Deep Learning-Based Technique for Driver Detection and Driver Assistance in Electric Vehicles with Better Performance. *Int. Trans. Electr. Energy Syst.* **2022**, 2022, 8548172. [\[CrossRef\]](#)
24. Selvaraj, D.C.; Hegde, S.; Amati, N.; Deflorio, F.; Chiasserini, C.F. An ML-aided Reinforcement Learning Approach for Challenging Vehicle Maneuvers. *IEEE Trans. Intell. Veh.* **2022**, 1–13. [\[CrossRef\]](#)
25. Ramshanker, A.; Chakraborty, S.; Elangovan, D.; Kotb, H.; Aboras, K.M.; Giri, N.C.; Agyekum, E.B. CO₂ Emission Analysis for Different Types of Electric Vehicles When Charged from Floating Solar Photovoltaic Systems. *Appl. Sci.* **2022**, 12, 12552. [\[CrossRef\]](#)
26. Hegde, S.; Bonfitto, A.; Rahmeh, H.; Amati, N.; Tonoli, A. Optimal Selection of Equivalence Factors for ECMS in Mild Hybrid Electric Vehicles. In Proceedings of the ASME 2021 International Design Engineering Technical Conferences and Computers and Information in Engineering Conference, Virtual Online, 17–19 August 2021; p. V001T01A019. [\[CrossRef\]](#)
27. Rajamani, R. *Vehicle Dynamics and Control*, 2nd ed.; Mechanical Engineering Series; Springer: New York, NY, USA, 2012.
28. Bonfitto, A. A Method for the Combined Estimation of Battery State of Charge and State of Health Based on Artificial Neural Networks. *Energies* **2020**, 13, 2548. [\[CrossRef\]](#)

29. Bonfitto, A.; Ezemobi, E.; Amati, N.; Feraco, S.; Tonoli, A.; Hegde, S. State of Health Estimation of Lithium Batteries for Automotive Applications with Artificial Neural Networks. In Proceedings of the 2019 AEIT International Conference of Electrical and Electronic Technologies for Automotive (AEIT AUTOMOTIVE), Torino, Italy, 2–4 July 2019; pp. 1–5. [\[CrossRef\]](#)
30. Subramanian, M.; Hoang, A.T.; Kalidasan, B.; Nižetić, S.; Solomon, J.M.; Balasubramanian, D.; C, S.; G, T.; Metghalchi, H.; Nguyen, X.P. A technical review on composite phase change material based secondary assisted battery thermal management system for electric vehicles. *J. Clean. Prod.* **2021**, *322*, 129079. [\[CrossRef\]](#)
31. di Napoli, M.; Galluzzi, R.; Zenerino, E.C.; Tonoli, A.; Amati, N. Investigation on the performances of a twin arm tensioning device. *Proc. Inst. Mech. Eng. Part D J. Automob. Eng.* **2019**, *233*, 1687–1697. [\[CrossRef\]](#)

Disclaimer/Publisher’s Note: The statements, opinions and data contained in all publications are solely those of the individual author(s) and contributor(s) and not of MDPI and/or the editor(s). MDPI and/or the editor(s) disclaim responsibility for any injury to people or property resulting from any ideas, methods, instructions or products referred to in the content.